Wavefield characteristics and coherency of seismic ground motion from a rocksite at argostoli Greece

Afifa Imtiaz, V. Perron, A. Svay, F. Hollender, P-Y. Bard, N. Theodoulidis

16th World Conference on Earthquake, 16WCEE 2017
Santiago Chile, January 9th to 13th 2017
Paper N° 1743
Registration Code: S-A1462971779

WAVEFIELD CHARACTERISTICS AND COHERENCY OF SEISMIC GROUND MOTION FROM A ROCKSITE AT ARGOSTOLI GREECE

A. Imtiaz[(1)], V. Perron[(2)], A. Svay[(3)], F. Hollender[(4)], P-Y. Bard[(5)], N. Theodoulidis[(6)]

[(1)] *Seismic Risk Engineer, Bureau de Recherches Géologiques et Minières (BRGM), France, a.imtiaz@brgm.fr*
[(2)] *Doctoral Candidate, CEA, DEN, F-13108 St Paul lez Durance Cedex, France, vincent.perron2@cea.fr*
[(3)] *Doctoral Candidate, IMSIA, University Paris-Saclay, France, angkeara.svay@centralesupelec.fr*
[(4)] *Researcher, CEA, DEN, F-13108 St Paul lez Durance Cedex, France, fabrice.hollender@cea.fr*
[(5)] *Researcher, University Grenoble Alpes, ISTerre / IFSTTAR, France, pierre-yves.bard@ujf-grenoble.fr*
[(6)] *Researcher, Institute of Engineering Seismology& Earthquake Engineering (ITSAK), Greece, ntheo@itsak.gr*

Abstract

The effects of spatial variation of earthquake ground motion (SVEGM) have been of great interest for a long time in the design and analysis of large and extended structures. In current engineering practices, the SVEGM is characterized by coherency functions, representing the degree of correlation between two ground motions, and usually estimated from the analysis of dense seismic arrays as an exponential decay with increasing frequency and interstation distance. However, most of these arrays are located at soil sites, resulting in very few coherency models for rock sites. In reality, many horizontally extended structures (e.g. bridges) may be supported at different site conditions - soil or rock or a combination of both. In order to extrapolate these models for different sites, it is imperative to characterize the loss of coherency based on some physical parameters, which requires identification of the different seismic phases contributing to the recorded signal. The current studies do not focus on such wavefield characterization, probably considering implicitly the ground motions on rocky sites to be minimally affected by the complex wave propagation. However, spatial incoherency has also been observed at rock sites owing to geological complexities such as weathering and shallow fracturation. In this context, this study analyzes the seismic events recorded from a dense array located on a rock site at Argostoli, Cephalonia Island, Greece. The array was installed within the framework of the ANR-PIA SINAPS@ project (www.institut-seism.fr/projets/sinaps/). The objective of the current study is to explore to what extent the non-direct, diffracted surface waves influence the seismic wavefield at a rock site and to investigate the loss of coherency of ground motions. The array consists of 21 velocimeters encompassing a central station in four concentric circles with diameters 20, 60, 180 and 360 m. The analyzed seismic dataset includes 40 events with magnitudes ranging from 2 to 5 and epicentral distance up to 200 km. MUSIQUE algorithm has been used to analyze the seismic wavefield by extracting the backazimuth and slowness of the dominant incoming waves and identifying the Love and Rayleigh waves. Lagged coherency has been estimated for all the available station pairs (max. 210 pairs per event) and the results have been averaged at different separation distance intervals (10-20, 20-30, 30-40, 80-90 m) for the entire dataset. The results were also compared with those from a similar array located on an adjacent small, shallow sedimentary valley. The analysis suggests that about 20% energy of the wavefield could be characterized as diffracted Love and Rayleigh waves, primarily arriving from the north-east and north-south directions, respectively. The spatial coherency estimations at the rock site are, generally, observed to be larger than those from the sedimentary array, especially at frequencies below 5 Hz. The directionality of coherency estimates observed from the soil array is absent in case of the rock array data. Comparison with the widely-quoted parametric models reveals that there is little correlation between the decay of coherency observed at the rock site and the models. The results clearly indicate the site dependent nature of the spatial incoherency as well as the locally generated wavefield at the rock and soil sites. The findings suggests that more rigorous studies based on rocky sites could definitely be instrumental in better understanding the causes of spatial variation of ground motion.

Keywords: Wavefield characteristics; Spatial Coherency; Dense Array; Rock Site; Cephalonia.

1. Introduction

The amplitude and phase variability observed between two adjacent ground motions are termed as the spatial variation of earthquake ground motion (SVEGM) and is attributed to the wave passage delay, spatial incoherence and local site effects. The effects of complex wave propagation and scattering, as the seismic waves encounter heterogeneities and irregularities along the source-to-site travel path and at the site, introduce significant variations in the ground motions over very short distances (within the dimensions of a large size engineering structure). Usually, these effects are considered to be less accountable for the rock type ground condition. Such sites are supposed to be stiffer and geologically more homogeneous, and the seismic wavefield is expected to be dominated by direct body waves. However, spatial incoherency has been observed at rock sites owing to weathering and cracking of the surficial rock formation [1]. Geological complexities of crustal structure have also been observed to be causing loss of coherency in ground motions [2]. This issue of site-to-site variability of differential ground motion could be particularly critical when the horizontally extended structures (e.g. bridges) are supported at different site conditions (soil or rock or a combination of both). Thus, when considering the infrastructure risk assessment, the spatial variability of ground motion should be investigated for both soil and rock sites.

In current engineering practices, the random phase variability due to incoherence effects is characterized by complex coherency functions from the stochastic analysis of dense seismic array data. However, most of these arrays have very large dimensions (>100 m) and are located mostly at uniform soil sites [3]. Hence, research on this subject has been mostly restricted to the soil site coherency models and is generally relevant for distances longer than the dimensions of large foundation structures. In current literature, very few coherency models have been developed for rock sites (e.g. [4–7]). Schneider *et al.* [8] compared coherency estimations from a set of rock and soil site arrays with the coherency function developed by Abrahamson *et al.* [9] based on a soil site data (LSST, Taiwan array) and for separation distance shorter than 100 m. The authors observed that the soil coherency fits well with the LSST model while the rock coherency yields comparable estimates when the site is not affected by topographic variations. Abrahamson [7] studied the same set of arrays but removed the ones affected by the topographic variations. The author compared the respective average coherency from the soil, soft-rock and hard-rock sites, and observed clear site dependence. At interstation distance 15-30 m, the coherency increases from soil to soft-rock and hard-rock sites whereas at 50-70 m the soil and soft-rock estimates become comparable and the hard-rock remains higher. Zerva and Stephenson [10] investigated seismic records from an array located on a variable site condition (on both valley and soft-rock) and observed that the complex wave propagation pattern affects not only the valley but also the surrounding soft-rock. The authors then highlighted the significance of irregular subsurface topography and formation of surface waves in the physical understanding of the spatial variation. Konakli *et al.* [11] estimated coherency from the USGS Parkfield rock array for the 2004 Parkfield mainshock and compared with the parametric models. Their result revealed that theoretical model of Luco and Wong [12] does not reproduce the observed variability of coherency decay rate with frequency and interstation distance. At smaller interstation distances (<100 m), the estimates were lower than those from the empirical model of Ancheta *et al.* [13], the updated LSST model, and the trend reverses at longer distances (>300 m). The authors concluded that the coherency at this site indicates a rather complex dependence on effects related to source, propagation, topography and site, and thus could not be explained by the general, simplified processes.

It is then imperative to characterize the loss of coherency on the basis of some physical features of the wavefield in order to explain the observations at a site and extrapolate them for other site conditions. However, this could be challenging due to the difficulties involved in identification and characterization of the different seismic phases contributing to the recorded signal. In addition, very little attention has been paid to the wavefield characterization of rock sites as they are considered to be minimally affected by complex wave propagation issues. The present study attempts to contribute to this area of research by analyzing the seismic events recorded from a dense array located on a rock site at Argostoli, Cephalonia Island, Greece. The objective of the study is to investigate to what extent locally generated diffracted surface waves influence the seismic wavefield at a rock site and to examine the site-dependence of the spatial variation, in other terms, whether the observed loss of

coherency is comparable to that from an adjacent soil site. The array was deployed by the SINAPS@ project and was operational from February 6 to March 10, 2014. It consists of total 21 broadband velocimeters, placed in four circles at diameters 20, 60, 180 and 360 m centered on a reference station. A set of 40 events containing events of local magnitude 2-5 occurring within the epicentral distance of 200 km was utilized to estimate the apparent propagation characteristics of the waves and to identify the energies carried out by Love and Rayleigh waves. The 'lagged' coherency was calculated to estimate the variability of random Fourier phase between all station pairs. Median coherency was obtained for four separation distance intervals (10-20, 20-30, 30-40, and 80-90 m) and compared with some widely-quoted parametric coherency models developed for rock and soil sites (e.g. [5,7,12,13]). This study also provides a unique opportunity to compare the results with those obtained from a similar dataset recorded at an array located on the adjacent sedimentary valley ([14,15]).

2. Dataset of Argostoli Rock Array

Located in the north-westernmost boundary of the Aegean plate, the Ionian Island of Cephalonia is considered to be the most active seismo-tectonic regions in Europe. The high seismicity of the area is associated with the dextral Cephalonia Transform Fault (CTF), situated in the northwestern boundary of the island. Two major earthquakes (moment magnitude M_w 6.1 and 6.0and hypocentral depth ~10 km) hit the area in January and February, 2014. These events were associated with the CTF and occurred within 20 km distance of the Argostoli town, damaging a significant number of engineering structures. They were also followed by a number of aftershocks up to M_w 5.5. A post seismic campaign was conducted at Argostoli within the framework of the SINAPS@ project, funded by the French Research Agency (ANR). A dense array, shown as Array R in Fig. 1(a), intended to study short distance spatial variability of ground motion, was deployed on the rock formation from February 6 to March 10, 2014. This network complements the dataset recorded by a geometrically similar, smaller-size array (Array A in Fig. 1 a) on the nearby small, shallow, sedimentary valley of Koutavos-Argostoli, operational from September, 2011 to April, 2012 by an EU-NERA (European Union - Network of European Research Infrastructures for Earthquake Risk Assessment and Mitigation) project [16]. The SINAPS@ array was implemented on a Cretaceous massive limestones (karstified and fractured) formation located about 2 km southeast of the NERA array (Fig. 1 a, b). The ensemble of the inverted shear (S-) wave velocity (V_s) profile of the rock array site from active and passive measurements has been provided in Fig. 1(c). On an average, the V_s reaches about 750 m/s at a depth around 10 m. Then it increases to about 1400 m/s at 60 m. The average velocity up to 30 m depth (V_{s30}) was estimated as 830±35 m/s.

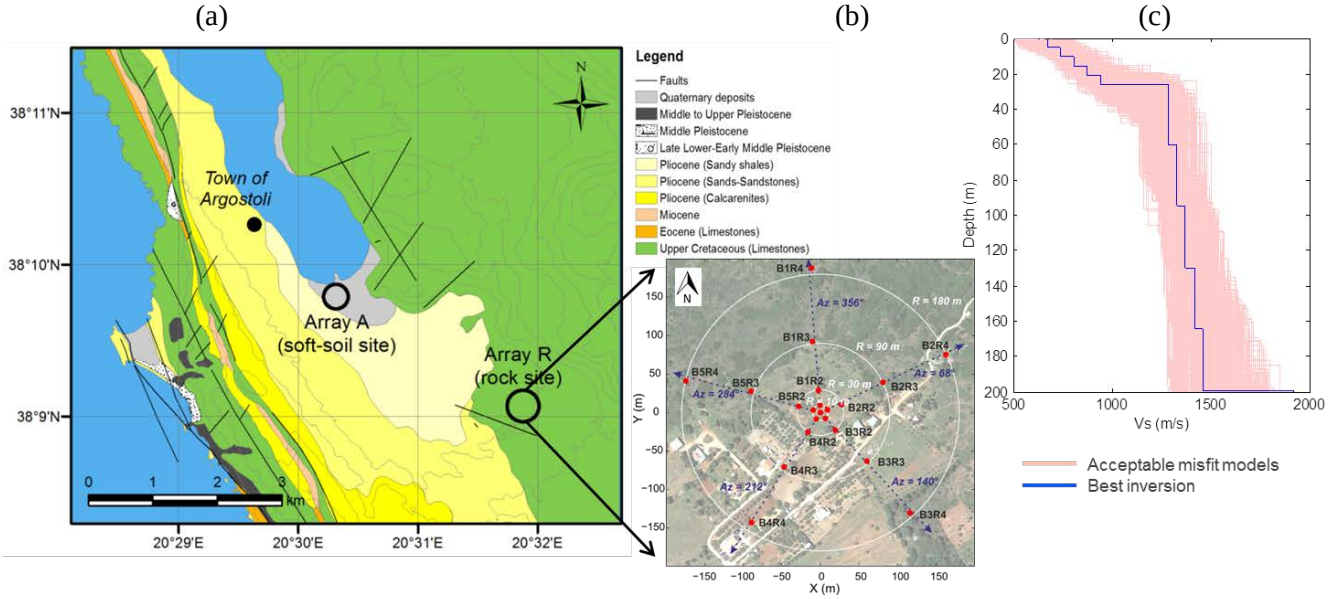

Fig. 1 – (a) Location of the Argostoli SINAPS@ rock array (Array R), and the NERA soil array [14,15]. (b) Layout of the Array R. (c) Ensemble of inverted shear wave velocity profile from the dispersion data obtained from active and passive measurements; the best inversion is given in blue and the 1000 "acceptable misfit" models are in light red.

The SINAPS@ 2D array consists of 21 three-component, broadband velocimeters. The stations are placed on the same geological unit, along four circles of diameters 20, 60, 180 and 360 m around the central station B0R0 (Fig. 1 b). On each circle, the stations branch off from B0R0 in N67°, N139°, N218°, N286° and N 356° directions. The network provided a rich database by recording nearly 2000 good quality earthquakes with local magnitude ranging from 1 to 4.7, at epicentral distances from 5 to 300 km, mainly corresponding to the seismic sequence of the aforementioned two consecutive earthquakes including some tens of events at greater distances and more varied azimuths [17]. A subset of 40 events with very good signal to noise ratio, local magnitude (M_L) 2 to 5, hypocentral depth (H) 4 to 40 km, epicentral distance (R_{epi}) 5 to 200 km, recorded by at least 20 stations of the array, was selected for the analysis. Table 1 summarizes the number of events by different groups and Fig. 2(a) shows their location. The entire seismogram was used for the wavefield analysis. On the other hand, the segment of signals beginning from the onset of the S-wave and representing mainly the S-phase duration (Fig. 2 b) was analyzed for the coherency estimation.

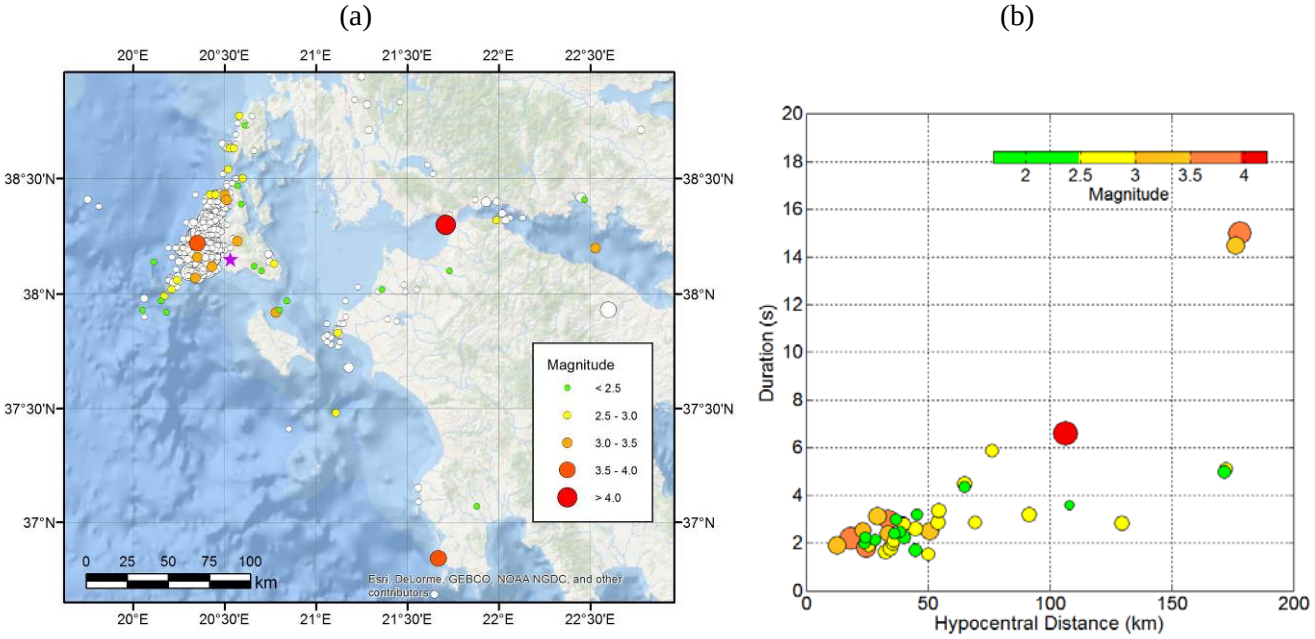

Fig. 2 – (a) Location of the selected events (in colored circles, with a diameter proportional to their magnitude). The purple 'star' marks the site and the white circles show the other available events in the database. (b) Duration of the selected time windows for coherency analysis.

Table 1 – Distribution of backazimuth, epicentral distance and magnitude of the selected dataset

Backazimuth quadrant	**Nb. of events**	**Epicentral Distance (km)**	**Nb. of events**	**Magnitude (M_L)**	**Nb. of events**
NE	11	0-30	9	~2-3	29
NW	12	30-60	19	3-4	10
SE	10	60-100	5	4-5	1
SW	7	100-200	7		
Total	40		40		40

3. Wavefield analysis and results

We have used the MUSIQUE algorithm [18] to perform the wave field characterization of the array data. MUSIQUE is a combination of the "classical" Multiple Signal Characterization (MUSIC) [19,20] and the quaternion-MUSIC [21,22] methods, that allows not only the extraction of backazimuth and apparent phase

velocity (or slowness) of the dominant waves crossing the array but also their characterization as Love or Rayleigh waves. Description of the algorithm for three-component signals is elaborated in [16,23]. We divided the entire length of signal into frequency dependent smaller time windows of five periods by considering 50% overlapping. From the array transfer function, the resolvable frequency range of Array R could be considered as 1-20 Hz for slowness > 0.0004 s/m. Therefore, we chose 200 log-based frequency steps between 1 to 20 Hz. The spectral averaging was done over five frequency samples centered on each frequency step. First, we retrieved the slowness and backazimuth (θ) of the most dominant wave crossing the array within each time-frequency signal block. Then the radial and transverse components were computed by projecting the east-west (EW) and north-south (NS) components of the signals along the identified θ and its orthogonal direction. We characterized a window as Love-dominant when the transverse energy and as Rayleigh-dominant when the summation of the radial and vertical energy was estimated to be more than 70% of the total window energy. If none of these criteria was fulfilled, no wave was identified for the time-frequency signal block under consideration.

During the post-processing, the results of the time-frequency blocks from each event containing window energy less than the median energy, signal to noise ratio less than 5 and slowness outside the range of 0.0004 to 0.008 s/m (apparent velocity 125 m/s to 2500 m/s) have been filtered out. A general description of the post-processing calculations could be found in [16]. Figure 3 shows an example of results for an M_L=3.5 earthquake (H = 31 km, R_{epi} = 13 km and backazimuth = N 348°). Fig. 3(a) displays the recorded velocity time series from the EW component of all the array stations. Fig. 3(b) shows histogram of the retrieved backazimuth distribution over the analyzed time windows and the colorbar corresponds to the window energy normalized by the squared Fourier amplitude. On this plot, we can follow the P and S wave arrivals and their respective durations through the energy concentration of the results. We can also observe that the energetic incident waves are arriving not necessarily from the source; they are rather scattered along other directions even during the early arrivals (<10 s). Figure 3(c) presents the 2D histogram of back-azimuth distribution over the analyzed frequencies. We have considered 72 grid points between 0° and 360° angles (interval = 5°) for the backazimuth axis and 31 log-based grid points between 1 and 20 Hz for the frequency axis in order to group the results. The red line marks the event's backazimuth and the colorbar is the summed normalized window energy of time-frequency blocks falling into the frequency-backazimuth intervals. The histogram outlines that over the entire frequency range, most of the energetic waves are appearing from north to north-east (roughly N330° to N35°), which corresponds mainly to the event's backazimuth direction. The scattered energies are observed from 6 to 15 Hz frequencies.

3.1 Diffracted wave field decomposition

In order to summarize the observations from all the events and to focus on the diffracted wavefield composition, the results corresponding to the direct arrivals (considered as back-azimuth ± 20°) were eliminated for each event. Then the estimates from all the individual events were summed up. Fig. 4(a) shows the summary of the backazimuth distribution of the diffracted waves from all the 40 events. The colorbar indicates the cumulative normalized energies. The scattered waves seem to be arriving mainly from the north-south direction over the entire frequency range. Fig. 4(b) and (c), respectively, represent the summary of the diffracted waves identified as Love and Rayleigh. Evidently, the diffracted Love waves arriving from the north-east direction contribute at frequencies up to 5 Hz whereas the Rayleigh waves from north-south direction contribute at the frequencies above 5 Hz. On an average, about 30% of the total analyzed energy (diffracted + direct) could be characterized as Love and Rayleigh waves, of which 20% corresponds to only diffracted surface waves (Fig. 4 d). Love wave composition is slightly higher up to ~2 Hz while Rayleigh wave is clearly more prominent in the frequencies above.

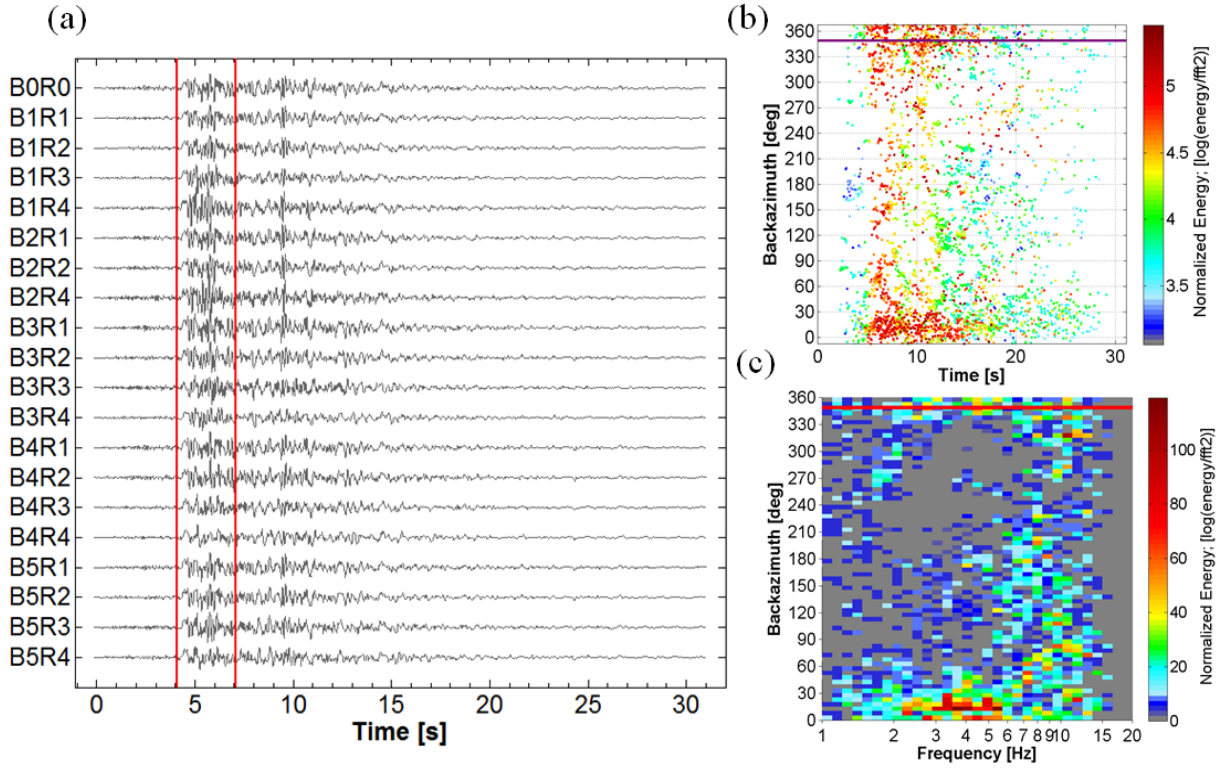

Fig. 3 – (a) EW component velocity time series recorded at the array stations for the event occurred on February 02, 2014 at 01:23:13 UTC (M_L = 3.5, Baz= N 348°, R_{epi} = 13 km, H=31 km). Entire signal length has been used for wavefield analysis and the segment between the red lines for coherency analysis. (b) Backazimuth distribution of the wavefield of the same event as a function of time. (c) 2D Histogram of the backazimuth as a function of frequency. Red line indicates the backazimuth of the event and colorbar the normalized energy.

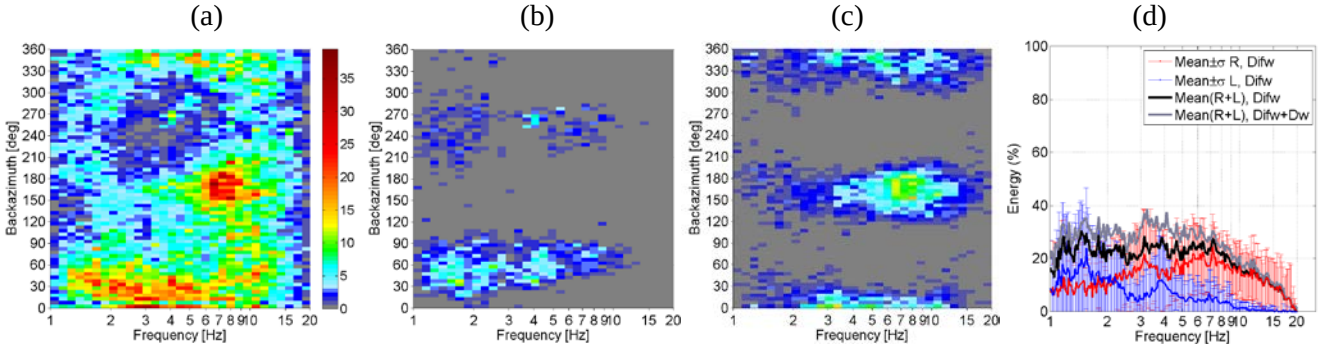

Fig. 4 – (a) Cumulative histogram of the backazimuth from the entire diffracted wavefield of 40 events after removing the contributions from the direct energies (Dw). Similar display for all diffracted waves identified as Love waves (b) and Rayleigh waves (c). Colorbar shows the sum of normalized energy. (d) Frequency dependence of the mean ±1σ proportion of diffracted energy (Difw) identified as Love and Rayleigh, with respect to the total analyzed energy (direct + diffracted).

4. Lagged Coherency analysis and results

4.1 Estimation of lagged coherency for a pair of stations

We calculated the lagged coherency where two time histories are aligned using the time lag that leads to the largest correlation of the motions in order to remove the so called wave passage effect. The duration of the probable S-wave window (Fig. 2 b), beginning from the onset of the wave, was selected by visually inspecting the records of the central station B0R0. The records from each station in the array were aligned with respect to B0R0. However, no remarkable time lag was observed among the records. The selected segments were cut and tapered by using 5% cosine bell window at both ends. The cross- and auto-spectra of the motions were calculated and averaged over 11 frequency points by using a Hamming (2M+1) window of smoothing as suggested by Abrahamson *et al.* [9]. For a 5.12 s long time window where frequency sampling is 50 Hz, the frequency smoothing corresponds to a bandwidth of 1.95 Hz. Finally, the lagged coherency at an interstation distance (ξ) has been estimated, over the cyclic frequencies (f) from 1 to 25 Hz, as the modulus of the complex coherency, the ratio between the smoothed cross spectrum $(\bar{S}_{jk})$ of the pair of stations (j, k), normalized by the geometric mean of the smoothed power spectra at the respective stations $(\bar{S}_{jj}, \bar{S}_{kk})$, and given by,

$$|\bar{\gamma}_{jk}(\xi, f)| = \frac{|\bar{S}_{jk}(f)|}{|\sqrt{\bar{S}_{jj}(f)\bar{S}_{kk}(f)}|} \quad (1)$$

The values of lagged coherency range from 0 to 1 for fully uncorrelated to fully correlated motions. When the interstation distance or frequency tends to zero the estimates tend to 1. Theoretically, at higher frequencies and larger interstation distances coherency tends to zero. However, in actual calculations the modulus of the complex coherency tends to a constant value rather than zero due to the level of smoothing applied to the inherent noise in the data. The median value of this constant is considered as 0.33 when an 11-point Hamming window is applied for frequency smoothing[24]. As the coherency estimates below this value are uninterpretable, we refer to this term as the resolvability threshold.

4.2 Summary of lagged coherency estimates from the dataset

As the variance of coherency estimates are frequency dependent, the statistical analysis is suggested on the ATANH ($\tanh^{-1}$) transformation of the estimates that produces approximately normally distributed data [9,25].The median resolvability threshold of lagged ATANH coherency is 0.34 when 11-point Hamming window is applied [24]. Imtiaz [15,16] analyzed the Array A data from a set of 46 events with similar characteristics (M_L 2-5 and R_{epi} up to 200 km) as those of Array R and showed that when the median coherency is derived by averaging all station pairs irrespective of their orientations, the two geometric horizontal components (EW, NS) as well as their rotation along any physical direction result in almost similar estimates. The authors also suggested that the source related parameters had negligible effect on the loss of coherency of the dataset. Therefore, we considered simply the EW and NS horizontal components for the coherency analysis and performed the averaging by considering all the events. We calculated the lagged coherency of the three components from all the pairs of stations available (max. 210 pairs per event) for the entire dataset. The 'individual median' and 'global median' of ATANH lagged coherency were estimated from all the pairs available for a single event and for the entire dataset, respectively, at different intervals of interstation distances. In order to present the results, we chose four ranges of interstation distance, 10-20, 20-30, 30-40 and 80-90 m, which included maximum number of station-pairs. Total 19, 15, 16 and 24 pairs per event are available, respectively, at the four interstation ranges when no station is missing in the data.

The median ATANH coherency of the entire dataset yield very similar values for all the three components. Therefore, we present the results in terms of the 'individual median' of each event (thin black curves) along with the 'global median' (thick red curve) of all events, as a function of frequency, from the data of EW component, in Fig. 5(a)-(d). A logarithmic scale is used for the frequency axis to highlight the results less

affected by the resolvability threshold. However, the estimated median curves are observed to be well above the threshold. The 'global median' from the Array A has also been plotted in thick blue curve. The rock coherency seems to be larger than that of the soil, at least up to 6 Hz at all interstation distances. However, it is observed to be slightly lower than the soil at higher frequencies and shorter separation distances (10-40 m).

Imtiaz [15,16] observed directional dependency of coherency estimates depending on the orientation of the station-pairs. Therefore, we compared the median estimates, by grouping the pairs in five array-branch directions (N356°, N67°, N139°, N213° and N286) with those (at N39°, N112°, N183°, N328° and N255°) coming from the Array A data. Example from the EW component coherency has been shown for two distance ranges in Fig. 6. While the directional variation of coherency is quite consistent at all separation distances for the soil data, no remarkable variation is observed for the rock array.

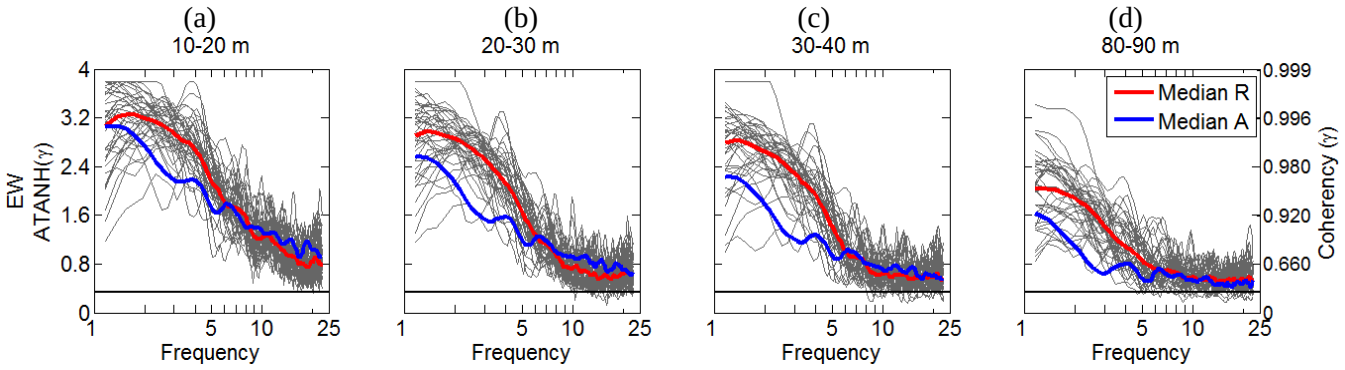

Fig. 5 – (a)-(d) Individual median EW ATANH coherency from each event (thin grey curves) and the global median ATANH coherency of all the 40 events (thick red curve) from the Array R. The blue curve shows the median obtained from 46 events recorded at the Array A. The corresponding lagged coherency values are marked at the right-side axis. Grey straight line marks the coherency resolvability threshold.

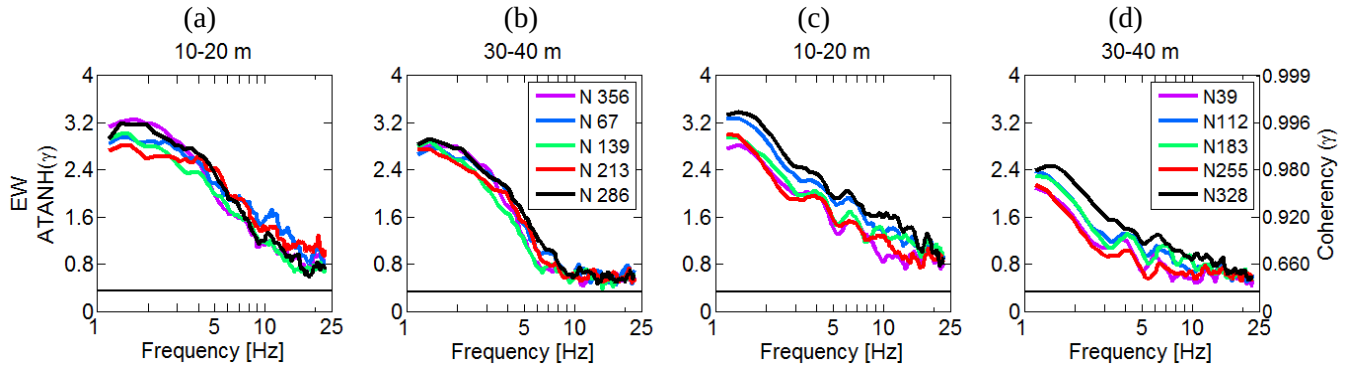

Fig. 6 – Median ATANH Coherency (EW component) along the five array branch directions of the (a)-(b) rock and (c)-(d) soil array.

4.3 **Comparison with existing parametric models**

A great variety of functional forms of coherency is available in the literature, though very few are based on rock data. We selected some widely quoted parametric models, two semi-empirical and two empirical, applicable for short interstation distances (<100 m), pertinent to soil and rock sites and compared with the median estimates from Argostoli data.

4.3.1. The parametric models

(a) The semi-empirical model of Luco and Wong [12] is based on the analysis of shear waves propagating through a random medium and expressed as a double exponential decay function of interstation distance (ξ) in m

and angular frequency (ω) in rad/sec,

$$|\gamma(\xi,\omega)| = \exp(-\alpha^2\omega^2\xi^2) \quad (2)$$

The coherency drop parameter is given by $\alpha = \nu/V_s$, where V_s is the average shear-wave velocity of the medium along the wave travel-path and ν is a constant related to the medium properties. Typical values of α are suggested within 2×10^{-4} to 3×10^{-4} sec/m. In this study, rather than estimating α from the dataset, we have considered the median value 2.5×10^{-4} sec/m.

(b) Menke *et al.* [5] derived one of the very few rock site coherency models, expressed as an exponentially decaying function of separation distance (ξ) in m and cyclic frequency (f) in Hz,

$$|\gamma(\xi,f)| = \exp(-\alpha f\xi) \quad (3)$$

where, α value is proposed within the range of 4×10^{-4} to 7×10^{-4} sec/m. We have considered the median, α = 5.5 × 10-4 sec/m.

(c) Abrahamson [7] proposed an empirical plane-wave coherency model for rock sites based on 78 earthquakes recorded at the Pinyon Flat array and expressed as,

$$|\gamma^{pw}(\xi, f)| = \left[1 + \left(\frac{f\tanh(a_1\xi)}{f_c(\xi)}\right)^{n_1(\xi)}\right]^{-1/2}\left[1 + \left(\frac{f\tanh(a_1\xi)}{a_2}\right)^{n_2}\right]^{-1/2} \quad (4)$$

The coefficients are given as: a_1=0.4, a_2=40, $n_1(\xi)$=3.8-0.04ln(ξ+1)+0.0105[ln(ξ+1)-3.6]^2, n_2=16.4 and f_c=27.9-4.82 ln(ξ+1)+1.24[ln(ξ+1)-3.6]^2 for the horizontal component; a_1=0.4, a_2=200, $n_1(\xi)$=2.03+0.41ln(ξ+1)-0.078[ln(ξ+1)-3.6]^2, n_2=10 and f_c=29.2-5.20 ln(ξ+1)+1.45[ln(ξ+1)-3.6]^2 for the vertical component. The plane-wave coherency is calculated by taking the real part of the smoothed cross-spectrum after aligning the ground motions on the best plane-wave speed. As such it includes the random variations in the wave passage effect and could be lower than the lagged coherency, especially at higher frequencies and longer interstation distances.

(d) Ancheta *et al.* [13] proposed a slight modification of the LSST model [9], based on 15 earthquakes on a soil site in Taiwan, and is given as,

$$|\gamma(\xi,f)| = \tanh\{(3.79-0.499\ln(\xi))[\exp[(-0.115-0.00084\xi)f]\frac{f^{-0.878}}{3} + 0.35\} \quad (5)$$

4.3.2. Results from the comparison

Fig. 7 shows the comparison of the average of two horizontal estimates from Argostoli data, in terms of coherency values, with the parametric models at four separation distance ranges. The models have been computed for interstation distances 15, 25, 35 and 85 m. Note that the semi-empirical and plane-wave coherency models approach zero at higher frequencies while the lagged coherency estimates and the empirical model tend to the resolvability threshold. Thus, they are not comparable at those frequencies. The rock coherency estimates seem to be in fair agreement with the models over all the frequencies at 10-20 m and up to 3 Hz at other distances. As interstation distance increases, the models tend to more overestimate the observations. The rock coherency estimates are always overestimated by the Abrahamson's hard-rock model. This is because Array R is situated on a softer rock formation compared to the data the model is based on. However, the soil model of Ancheta *et al.* also overestimates the rock data at all the distances above 20 m. One fundamental issue with the semi-empirical models is that they consider a constant decay rate with the wavelength whereas the real data exhibit varying decay tendencies with respect to frequency and interstation distance. Therefore, we observe that the double exponential decay of Luco and Wong fits very well with the rock estimates at 80-90 m (up to about 6 Hz) but not at shorter interstation distances. It seems that the coherency from data decays much faster at shorter distances. This issue is taken care of in the empirical models but the overall decay rate in the data still remains

higher than the models. The coherency estimates from the Argostoli soil array seems to be relatively poorly presented by all the models. However at shorter interstation distances (up to 40 m) and higher frequencies (>5 Hz) the rock estimates yield slightly lower values than the soil ones. As the soil array is located on a uniform site, effects from topographic variation could be contributing to the lower coherency values of the rock data.

Regarding the vertical coherency, similar conclusions could be drawn for rock array data (Fig. 8). However, the vertical coherency from soil array seems to be decaying at a much faster rate up to about 7-8 Hz and shows a reverse tendency afterwards, especially at shorter interstation distances (10-40 m). This increasing trend is totally absent in the rock data. It could be argued that, the vertical coherencies at the soil site seem to be augmented by the presence of converted S-P waves or Rayleigh waves with higher phase velocities at high frequencies.

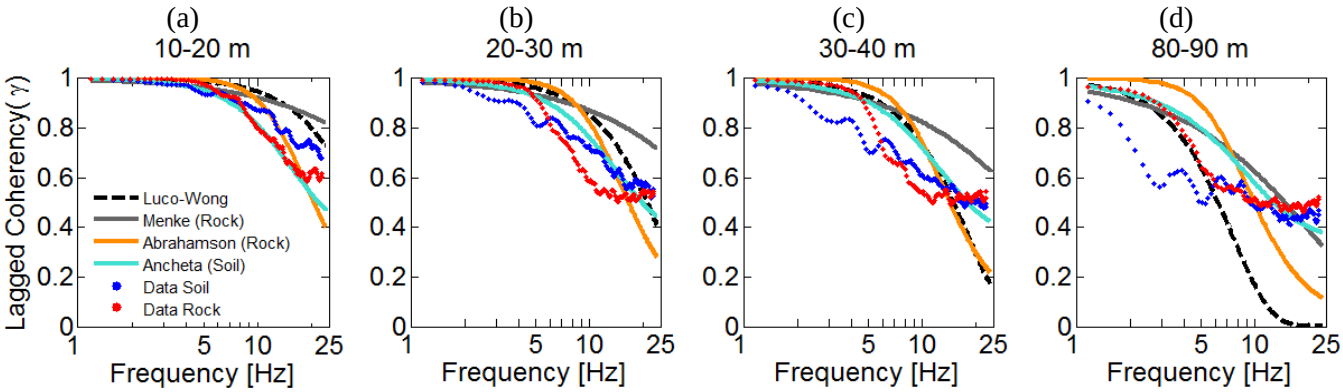

Fig. 7 – Comparison of the horizontal component median coherency estimated from Argostoli rock and soil array with the existing semi-empirical and empirical coherency models.

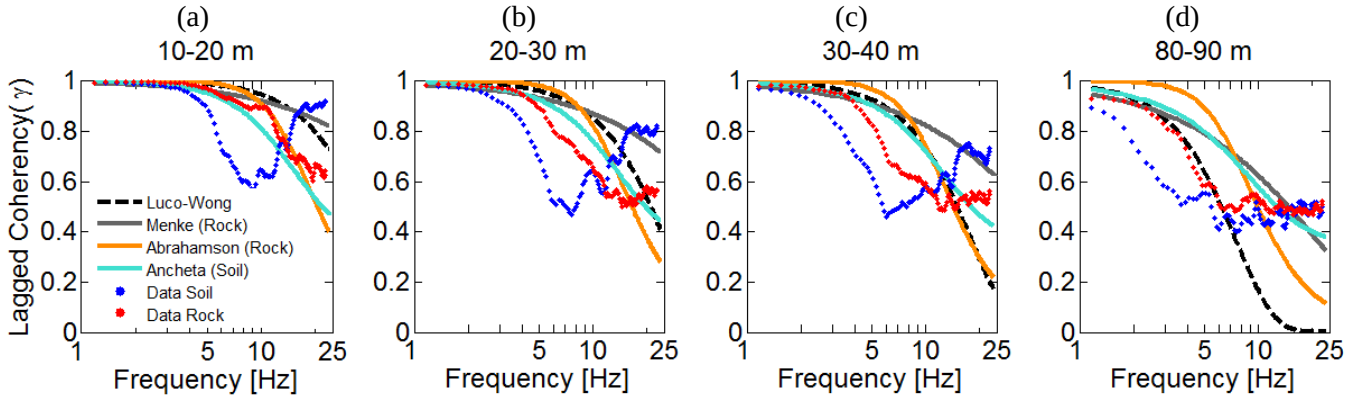

Fig. 8 – Comparison of the vertical component median coherency estimated from Argostoli rock and soil array with the existing semi-empirical and empirical coherency models.

5. Discussion and Conclusions

The current study performs a twin analysis of wavefield characterization and spatial incoherency of seismic motion recorded at a dense array of stations on a rock site. A large number (40) of small to moderate, shallow, local and regional events distributed around the site were analyzed. The loss of coherency was estimated for interstation distance ranging from 10 to 360 m. The median of the estimates at different interstation distance ranges (<100 m) have been examined and compared with those estimated from a similar dataset recoded at a nearby soil site as well as with some of the existing parametric models. The key results derived from the first part of the work, that is, the analysis of composition of the wavefield, reveal that some wave scattering over the frequency range of 1-20 Hz is arriving from the north-south and north-east directions of the site for almost all events whatever their actual backazimuth. However, analysis of the energy carried by those diffracted waves

reveal that on an average, only 20% of the total analyzed energy is associated to diffracted Love and Rayleigh waves. Imtiaz *et al.* [14] reported from the study on the nearby soil array that about 40-60% of the analyzed seismogram energy could be characterized as diffracted surface waves associated to 2D or 3D geometrical effects, appearing mainly from the valley-edge directions, with clear frequency-dependent dominance of Love and Rayleigh waves. Hence, it is evident that the formation of diffracted surface waves is much more significant on the sedimentary valley and may play an important role in causing loss of coherency and its directional variability.

In the second part of the work, our estimated median coherency from the rock data shows very similar decaying tendencies for all the three components; it is also found to be, generally, higher than that from a nearby soil site. However, at shorter interstation distances and higher frequencies the rock coherency exhibits slightly lower values than that of the soil. This could be attributed to a number of factors including the presence of weathered or relatively lower velocity surficial layer, topographic variation or larger heterogeneities in the subsurface geology. Further investigation is suggested to better understand this unexpected observation and identify its origin. The directional variability of coherency, depending on the orientation of the station-pairs, observed in the soil data appears to be negligible for the rock. Moreover, the vertical coherency from the rock site seems to be comparable with the horizontal which is not the case for the soil site. The comparison with the empirical models does not show any consistent correlation with the observations. Overall, the rock coherency is overestimated by all the parametric models even by the empirical one based on the soil data. Apparently, the decay rate of coherency as a function of frequency seems to be not only site dependent but also interstation distance dependent. The faster decay rate from the Argostoli data (both soil and rock) is not well-captured by the empirical models. On the other hand, the variability in the decay rate, especially with respect to the interstation distance, is not addresses by the semi-empirical models. The findings of the present work have important implications emphasizing the site dependent nature of spatial variation, and the difficulty to extrapolate an empirical model from one site to another. However, there is abundant room for further progress; more efforts should be undertaken on analyzing the spatial variability of ground motions on rock sites not only to better understand the short-distance spatial variation but also to include them in current engineering models.

6. Acknowledgements

This work was carried out under the SINAPS@ project that receives French funding managed by the National Research Agency under the program “Future Investments” (Sinaps@ reference: ANR-11-RSNR-0022). Sinaps@ is a “Seism Institute” project (http://www.institut-seism.fr/en/). We would like to thank all the contributors of this work (especially for help on the field during the Sinaps@ post-seismic campaign): Régis Cottereau (ECP), Cécile Cornou (ISTerre), Marc Cushing (IRSN), Alberto Frau (CEA/EMSI), Sébastien Hok (IRSN), Philippe Langlaude (CEREMA), Aurore Laurendeau (CEA/LDG), Armand Mariscal (ISTerre) and Alexandros Savvaidis (EPPO-ITSAK); as well as our local help on the Cephalonia Island: Agis Konidaris (TEI) and Chrisostomos Andreou.

7. References

[1] Steidl JH, Tumarkin AG, Archuleta RJ (1996) : What is a reference site? *Bull. Seismol. Soc. Am.*, 86, 1733–1748.

[2] Somerville PG, McLaren JP, Sen MK, Helmberger DV (1991) : The influence of site conditions on the spatial incoherence of ground motions. *Struct. Saf.*, 10, 1–13. doi:10.1016/0167-4730(91)90003-R.

[3] Zerva A, Zervas V (2002) : Spatial variation of seismic ground motions: an overview. *Appl. Mech. Rev. ASME*, 55, 271–297.

[4] Cranswick E (1988) : The information content of high-frequency seismograms and the near-surface geologic structure of “hard rock” recording sites. *Pure Appl. Geophys. PAGEOPH*, 128, 333–363. doi:10.1007/BF01772604.

[5] Menke W, Lerner-Lam AL, Dubendorff B, Pacheco J (1990) : Polarization and coherence of 5 to 30 Hz seismic wave fields at a hard-rock site and their relevance to velocity heterogeneities in the crust. *Bull. Seismol. Soc. Am.*, 80, 430–449.

[6] Toksoz MN, Dainty AM, Charrette III EE (1991) : Spatial variation of ground motion due to lateral heterogeneity. *Struct. Saf.*, 10, 53–77.

[7] Abrahamson NA (2007) : Program on Technology Innovation: Effects of Spatial Incoherence on Seismic Ground Motions. *EPRI, Palo Alto, CA 2007. 1015110*.

[8] Schneider JF, Stepp JC, Abrahamson NA (1992) : The spatial variation of earthquake ground motion and effects of local site conditions. *Proc. Tenth World Conf. Earthq. Eng., A. A. Balkema, Rotterdam* : pp. 967–972. http://www.iitk.ac.in/nicee/wcee/article/10_vol2_967.pdf.

[9] Abrahamson NA, Schneider JF, Stepp JC (1991) : Empirical Spatial Coherency Functions for Application to Soil-Structure Interaction Analyses. *Earthq. Spectra*, 7, 1–27. doi:10.1193/1.1585610.

[10] Zerva A, Stephenson WR, (2011) : Stochastic Characteristics of Seismic Excitations at a Non-Uniform (Rock and Soil) Site. *Soil Dyn. Earthq. Eng.*, 31, 1261–1284.

[11] Konakli K, Der Kiureghian A, Dreger D (2014) : Coherency analysis of accelerograms recorded by the UPSAR array during the 2004 Parkfield earthquake. *Earthq. Eng. Struct. Dyn.*, 43, 641–659. doi:10.1002/eqe.2362.

[12] Luco J, Wong H (1986) : Response of a rigid foundation to a spatially random ground motion. *Earthq. Eng. Struct. Dyn.*, 14, 891–908.

[13] Ancheta TD, Stewart JP, Abrahamson NA (2011) : Effects of Surface Geology on Seismic Motion. *4th IASPEI / IAEE Int. Symp*. Univ. Calif. St. Barbar., California .

[14] Imtiaz A, Cornou C, Bard P-Y, Hobiger M (2014) : Diffracted Wave Field And Coherency Analysis: An Example From Dense Array Network In Argostoli Basin, Cephalonia, Greece. *Second Eur. Conf. Earthq. Eng. Seismol.(2ECEES)*, Istanbul, Turkey, . doi:10.13140/2.1.2274.7528.

[15] Imtiaz A, Cornou C, Bard P-Y, Zerva A (2015) : Spatial coherence of seismic ground motion and geometric structure of the sub-surface: an example in Argostoli, Greece. *9th Colloq. Natl. AFPS 2015*, Marne-La-Vallée, France, . https://hal-brgm.archives-ouvertes.fr/hal-01226818/ (accessed May 14, 2016).

[16] Imtiaz A (2015) : Seismic wave field, spatial variability and coherency of ground motion over short distances : near source and alluvial valley effects. *Université Grenoble Alpes*. https://tel.archives-ouvertes.fr/tel-01148138/ (accessed May 14, 2016).

[17] Hollender F, Perron V, Imtiaz A, Svay A, Mariscal A, Bard P-Y, Cottereau R, Lopez-Caballero F, Cushing M, Theodoulidis N, Moiriat D (2015) : Close to the lair of Odysseus Cyclops : the SINAPS@ postseismic campaign and accelerometric network installation on Kefalonia Island. *9th Colloq. Natl. AFPS 2015*, Marne-La-Vallée, France .

[18] Hobiger M, Le Bihan N, Cornou C, Bard P-Y (2012) : Multicomponent Signal Processing for Rayleigh Wave Ellipticity Estimation Application to Seismic Hazard Assessment. *IEEE Signal Process. Mag.*, 29, 29–39–29–39.

[19] Schmidt RO (1986) : Multiple emitter location and signal parameter estimation. *IEEE Trans. Antennas Propag.*, 34, 276–280–276–280.

[20] Goldstein P, Archuleta RJ (1987) : Array analysis of seismic signals. *Geophys. Res. Lett.*, 14, 13–16. http://dx.doi.org/10.1029/GL014i001p00013.

[21] Miron S, Le Bihan N, Mars J (2006) : Quaternion-MUSIC for vector-sensor array processing. *IEEE Trans. Signal Process*, 54, 1218–1229–1218–1229.

[22] Miron S, Le Bihan N, Mars J, (2005) : High resolution vector-sensor array processing using quaternions. *IEEE Int. Conf. Stat. Signal Process. Bordeaux, Fr*.

[23] Hobiger M (2011) : Polarization of surface waves : characterization, inversion and application to seismic hazard assessment. *Université de Grenoble*. https://tel.archives-ouvertes.fr/tel-00577887/ (accessed May 14, 2016).

[24] Abrahamson NA (1992) : Spatial Variation of Earthquake Ground Motion for Application to Soil-Structure Interaction. *Final Report, EPRI TR-100463, Tier 2, RP 2978-1*.

[25] Harichandran RS (1991) : Estimating the spatial variation of earthquake ground motion from dense array recordings. *Struct. Saf.*, 10, 219–233.